

Paper Ref: acp-2020-456

Title: " Determination of the absorption cross-sections of higher order iodine oxides at 355 nm and 532 nm"

### RESPONSE TO THE REPORT OF REVIEWER #3

We are grateful to the reviewer for helpful and constructive comments and suggestions. We address them point by point below. The Reviewer's comments are shown in bold typescript, our response in normal typescript. Changes to the manuscript are highlighted in red. Page numbers refer to the revised manuscript.

**The manuscript by Lewis et al. (acp-2020-456) describes experimental measurements and theoretical calculations to determine the absorption cross sections of higher iodine oxides, as well as modeling to assess the impact of the photochemistry in the atmosphere. The quality of the experimental data for what appear to be challenging experiments is reasonable. I have concerns that the modest theoretical methods applied may be inadequate to describe the electronically excited states in molecules such as the iodine oxides, but that is somewhat beyond my area of expertise. If the authors could demonstrate clearly that they are capable of reasonably predicting molecular properties of a well-known iodine oxide, it would go some way to assuaging those concerns.**

Following the suggestion of the reviewer, we have compared the experimental absorption spectra of IO, OIO and HOI with the corresponding spectra calculated with the TD-DFT method. This comparison is shown in Figure A2 (below). It can be seen that even for radicals like IO and OIO, the method gives a reasonable prediction of the spectral position of the electronic bands, and average absorption cross sections of the same order. For closed-shell molecules, the agreement is expected to be better, as demonstrated for HOI.

We have introduced the following sentence in Page 10, at the end of section 2.2: **Although there are more advanced methods for the calculation of electronic spectra, TD-DFT offers a reasonable compromise between low computational cost and accuracy of the predicted transitions. Figure A2 shows a comparison between the experimental and TD-DFT absorption spectra of IO, OIO and HOI. Note that although the TD-DFT method is not designed to predict ro-vibrational structure, the spectral positions of the electronic bands and the average absorption cross sections are in reasonable agreement with the experiment, even in the case of**

open shell species like IO and OIO. Higher iodine oxides are closed shell molecules and the accuracy of the transitions is expected to be similar to the result for HOI.

The new figure included in the Appendix A (Figure A2) is the following:

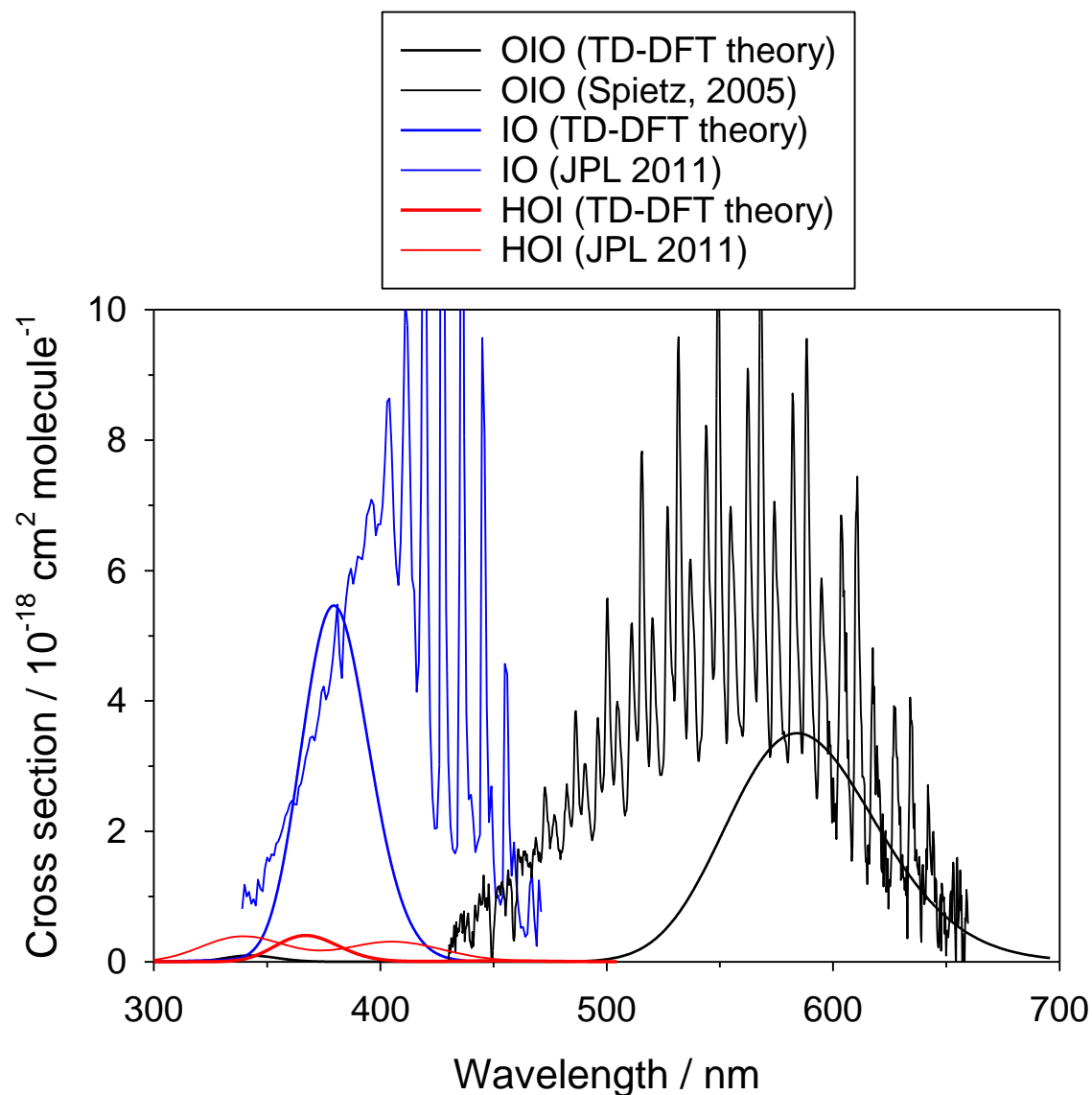


Figure A2: Experimental absorption cross sections of IO (Sander et al., 2011), OIO (Spietz et al., 2005) and HOI (Sander et al., 2011) and absorption spectra calculated with the TD-DFT method (this work).

**I am unable to comment on the atmospheric modeling, although I would note that they rely on cross sections that have been determined experimentally at only two wavelengths.**

Even though the experiments are limited to two wavelengths, this is significant progress with respect to what was known before. We use the two single-wavelength experimental cross sections to show that spectra measured by absorption spectroscopy cannot be directly used in

the determination of photolysis rates and to validate calculated spectra, which do not suffer from absorption overlap issues. Of course, future studies should address experimentally the wavelength dependence of the absorption spectra of iodine oxides, e.g. by using the same approach presented in our work but with a tunable laser instead of a Nd:YAG laser.

**The paper is, for the most part, fairly well-written although the structure could be improved. Some of the text in the methods section would be better located in the results section. For example, lines 144-179 (including Figure 3 and 4) describe measurements, not the experimental set-up, and belong in the results section, as do the results of the ab initio calculations.**

This paper is not concerned with demonstrating the observation of  $I_xO_y$  by PI-ToF-MS, which has been already reported in previous publications. Since this method of detection of  $I_xO_y$  is already proven, we do not think that Figure 3 belongs to the results section, but rather to the methods section as a proof that we can see these species.

We have introduced the following sentence in Page 6, Line 137: **Successful detection of  $I_xO_y$  by this method has been demonstrated elsewhere (Gomez Martin et al., 2013; Wei et al., 2017; Gomez Martin et al., 2020).**

Similarly, Figure 4 and the corresponding discussion also deal with methodological considerations rather than with new results. The use of PI-TOF-MS in photochemical experiments has been discussed previously (Baeza-Romero et al, 2012). New text has been inserted in p. 8 after Figure 4 in response to another concern of the reviewers (see below), which further helps to appreciate the methodological nature of this section of the paper.

Regarding the ab initio calculations, we consider the determination of the ground state geometries and molecular parameters of iodine oxides as merely methodological, since there are previous publications where these have been reported at different levels of theory.

Insertion in p. 10, L245: **Note that the ground states some of these oxides have been studied at a higher level of theory elsewhere (Kaltsoyannis and Plane, 2008; Galvez et al., 2013)**

The novelty of these ab initio calculations is the determination of absorption spectra. We have added a new subsection 3.3 where the ab initio spectra are formally mentioned as results, and additional information about the spectra is provided.

Addition in Page 16:

### 3.3. Ab initio spectra

The calculated spectra are displayed in Figure 9 ( $\text{I}_2\text{O}_2$ ,  $\text{I}_2\text{O}_3$  and  $\text{I}_2\text{O}_4$ ), Figure 10 ( $\text{I}_3\text{O}_6$  and  $\text{I}_3\text{O}_7$ ), and Figure 11 ( $\text{IO}_3$ ). Oscillator strengths of the electronic transitions that are responsible for the visible and UV absorptions are provided in Appendix A. The TD-DFT spectra were wavelength-shifted by applying a constant energy shift to get agreement with the experiment at 355 nm. The shifts are quite modest, within the expected error at this level of theory (Foreman and Frisch 2015):  $\text{I}_2\text{O}_3$  (30 kJ mol<sup>-1</sup>),  $\text{I}_2\text{O}_4$  (-12 kJ mol<sup>-1</sup>),  $\text{I}_3\text{O}_6$  (9.2 kJ mol<sup>-1</sup>),  $\text{I}_3\text{O}_7$  (-21 kJ mol<sup>-1</sup>). Applying a constant energy shift means assuming that all the excited state energies are offset by a constant amount with respect to the ground state.

**Table 1 compiles calculated geometries and vibrational frequencies, which are of little relevance to the subject matter of the paper and could be readily removed to supplementary information. On the other hand, no data for the calculated energies or oscillator strengths of the electronically excited states that are responsible for the visible and UV absorption are provided; the calculated ionization energy is also reported for only one species ( $\text{IO}_3$  on line 257). These data impact directly on the interpretation of the experimental results and should be compiled either in a revised version of Table 1 or in supplementary information.**

Table 1 and Figure 5 have been removed from the main text and are now included in Appendix A following the reviewer request. The calculated oscillator strengths have been included in Appendix A as well.

Calculated and experimental ionization energies of  $\text{I}_x\text{O}_y$  species relevant to this work (except  $\text{IO}_3$ ) have been reported previously, and the corresponding papers (Gómez Martín et al., 2013; Wei et al., 2017; Gómez Martín et al., 2020) are properly cited in the paper (page 6).

**The results section would benefit from a clearer introduction to describe what  $\text{I}_x\text{O}_y$  species are detected in the experiment and their time dependence. A figure showing the different “kinetic profiles”, which are alluded to, would also be valuable. Presumably, the profiles have been characterized by varying the delay between the 248 nm photolysis pulse used to initiate the chemistry and the VUV photoionization pulse.**

Why have clarified the species detected and the meaning of the “kinetic profiles” in the experimental section. Another wording for the same concept is “time trace”. The reviewer is

correct in that time is defined as the delay between excimer photolysis and VUV photoionization.

Changes in Page 7, Lines 175-160: Each experiment results in a 3-dimensional dataset of signal intensity (proportional to concentration) vs. 248 nm photolysis - VUV photoionization delay time (kinetic profile or time trace) and time-of-flight (mass spectrum). Figure 3 shows mass spectra with the most prominent peaks obtained at different delay times. Mass-to-charge (m/z) calibration of time-of-flight was performed by selecting a number of well-known prominent mass peaks (e.g. IO at m/z =143, OIO at m/z =159, I2O3 at m/z =302, I2O4 at m/z =318 and I3O7 at m/z =493 (Gómez Martín et al., 2013)).

We now refer specifically to Figure 3 in the results section to make clearer what are the target species in the context of the mass spectrum. We have added a better introduction to the Results section, moving here some material from the Methods section describing how fragmentation problem affects our results and adding the requested figure with kinetic profiles:

As described in the experimental section, kinetic profiles of the growth and removal of the target iodine oxide species shown in Figure 3 were carried out in order to define the time periods with the most suitable kinetic profiles for photolysis measurements (Figure 5). Fragmentation of iodine oxides was a significant problem in these experiments, as predicted from ionization energy calculations of larger iodine oxides to possible photofragments at 10.5 eV (Gomez Martin et al., 2020). High amounts of active iodine ( $\text{IO}_x = \text{I}, \text{IO}$ ) released from reaction R12 lead to fast formation of  $\text{I}_x\text{O}_y$  and particles. Under these conditions, at long times after the peak IO and OIO (~3-5 ms), the observed signal of IO, OIO and  $\text{I}_x\text{O}_y$  is contaminated by photofragmentation of higher order iodine oxides. For this reason, great care needed to be taken to establish a time window for each species wherein higher oxides are not present, to ensure that any depletion in the mass spectrometric signal for each species is exclusively due to the removal of the species via photolysis (Figure B1). Evidence of fragmentation comes in the form of a secondary growth in the signal seen for IO and OIO (Figure 5). The delay between the excimer and the Nd:YAG photolysis laser was therefore carefully selected to coincide with a period of relatively constant signal of the desired analyte, typically a maximum for short lived species, or a slow rise for larger reaction products of interest.

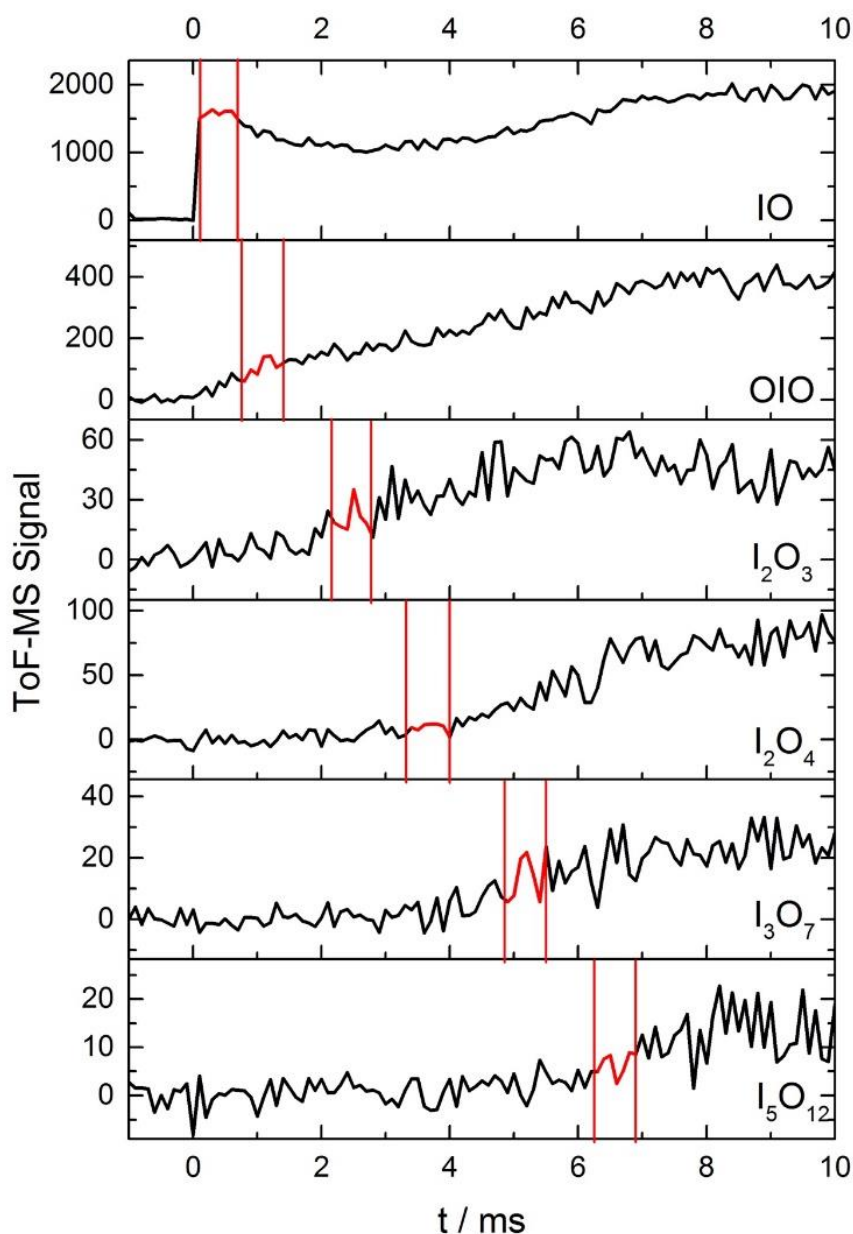


Figure 5: Time traces of IO, OIO,  $I_2O_3$ ,  $I_2O_4$ ,  $I_3O_7$  and  $I_5O_{12}$  from -1-10 ms, at 1 ms intervals for a mixture of He (10 torr),  $O_3$  and  $I_2$  ( $[O_3] = 4 \times 10^{14}$  molecule  $cm^{-2}$   $[I_2] = 2.8 \times 10^{14}$  molecule  $cm^{-2}$ ) flash photolyzed by an excimer pulse at  $t = 0$  (130 mJ pulse $^{-1}$ ). The red sections highlighted for each species correspond to the optimal delay windows for photolysis of the corresponding species for this set of conditions.

Kinetic profiles of IO, OIO,  $I_2O_3$ ,  $I_2O_4$ ,  $I_3O_7$  and  $I_5O_{12}$  are shown in Figure 5, along with 0.5 ms windows within which each species can be photolysed free of contamination from daughter ions of larger  $I_xO_y$  species. To further illustrate the lack of contamination from higher oxides, the mass spectra collected during the windows outlined in the kinetic traces are averaged, showing the target species to be present absent of higher oxides (new Figure B1). The reviewer is correct to assume that contribution to a signal of interest from daughter ions of larger  $I_xO_y$  species would cause erroneous measurement of photodepletion in the species of interest, and as such, great care was taken to eliminate the possibility of the aforementioned contamination.

Note that the kinetic traces were obtained at the beginning of each experimental session, for each set of conditions, in order to elucidate the optimal time delay for a species of interest, whereby the signal was present, but not larger species, the daughter ions of which would contaminate the desired signal. The kinetic trace was generally not averaged for a long period of time, since good signal to noise is not required, and is just a preliminary check used to establish the correct timings for the photolysis experiments. This discussion appears now in Appendix B:

### **APENDIX B. Photofragmentation of $I_xO_y$ species**

The photofragmentation of  $I_xO_y$  species to daughter ions in the photoionization chamber of the detection apparatus necessitates careful experimentation in order to ensure that any photodepletion of a species of interest is solely due to its 355 nm or 532 nm photolysis in the flow tube, and not obscured by the daughter ions of larger  $I_xO_y$  species. To elucidate the optimal window for investigating photodepletion of each species, time resolved mass-spectra were recorded for each set of experimental conditions (Figure 5). From the kinetic information, it is then possible to inspect the averages of the mass spectra within these windows to ensure that the species of interest is present, but larger  $I_xO_y$  species are not, as shown in Figure B1. By ensuring no larger  $I_xO_y$  species are present, it follows that for a species of interest, only parent ions of the species are contributing to the signal intensity within that time window, and that no contribution to the recorded signal is coming from daughter ions. Note that the signals shown in Figure 5 and Figure B1 are not accumulated for extended periods of time, and as such are relatively noisy. Long accumulation times and corresponding large signal to noise ratios are unnecessary for these experiments, since the objective is simply to elucidate optimal time-delays within which photodepletion experiments are carried out, (photodepletion experiments are typically carried for  $\sim 10\times$  as many accumulations) and are carried out prior to an experimental session. It should be noted also that the optimal timescales such as those shown in Figure 5 and Figure B1, vary depending on the concentration of IO formed at the beginning of the reaction sequence, and since the reactions which facilitate the stepwise formation of the higher oxides are second-order, even modest changes in [IO] at early times can result in significant changes to the appearance times of the different species of interest.

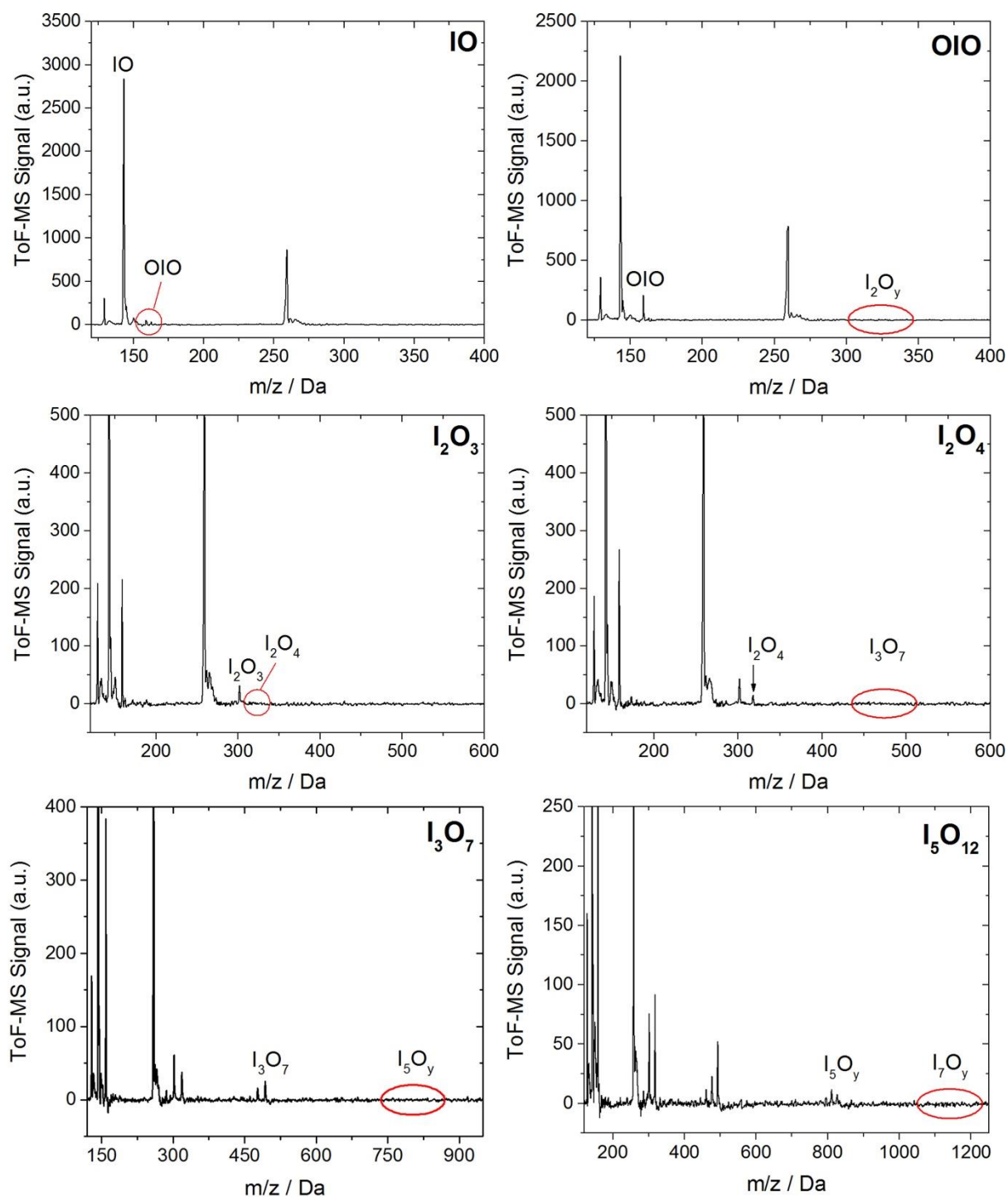


**Figure B1:** Mass spectra corresponding to the optimised time delays shown in Figure 5. The plots are generated by averaging the signal obtained for each mass over the 5 ms window. The species of interest is given in the top right corner of each spectrum.

The authors acknowledge (pages 13, 14) that fragmentation of larger species, can lead to signal increases at the masses of the photofragments, which would lead to possible systematic under-estimation of the depletion. To use the authors' example of I3O7, I have no sense of how much is present at the 7.6 ms time delay when the I2O4 (a potential daughter signal) is measured. Could other experimental parameters be varied (in

**principle) to modify the relative yields of different IxOy species to explore this in more detail? Relative photoionization cross sections for the various species will also play a role.**

This question is answered in conjunction with the previous question in the above response, and has been clarified with the aid of new figures in the main text and Appendix B.

**The depletion measurements in Figure 6 and 7, as well as the NO2 depletion used for actinometry in Figure 4, are shown with an overlaid empirical fit. However, the fitting function is not described, or its choice explained, nor are any reasons for the different shapes discussed. Why does the effective “width” of the drop off appear to change for different species? Is it even meaningful? What delay does the time axis correspond to in these figures? The experiments use three laser pulses (two photolysis pulses, one to initiate the chemistry and a second to dissociate the iodine oxides) and one to detect the IxOy species. Clarity about which exactly which delay is being referred to would be helpful.**

These points have been raised by Reviewers #1 and #2 as well. A detailed answer can be found in the response to Reviewer #1. We added the following piece of text to the manuscript to answer the reviewers’ concerns:

Insertion in Page 8, Line 196: **The trace shown in Figure 4, which is similar to all the traces obtained in this experiment, exhibits a delay between the pre- and post-photodepleted signal. This delay corresponds to an instrumental sampling time depending on the alignment of the lasers and the molecular masses of the bath gas and the sample species (Baeza-Romero et al., 2012). In the present experiments, it was necessary to leave a small gap (~2 mm) between the photolysis volume and the sampling pinhole, so as to avoid hitting the skimmer cone with the laser. The diffusional exchange of molecules between the photodepleted volume, and the un-photodepleted volume immediately before the pinhole blurs the onset of the photodepletion as it is measured by the TOF-MS. The values of  $S_0$  and  $S_1$  were obtained by empirically fitting the photodepletion trace to a sigmoidal function:**

$$y = S_0 + \frac{S_1 - S_0}{1 + 10^{(\log x_0 - x)p}} \quad (2)$$

**Fitting to this function ensures that the flat sections corresponding to the pre- and post-photodepletion concentrations ( $S_0$  and  $S_1$  respectively) are characterized in the precise regions outside of the aforementioned “blurred” zone. The parameters  $x$  and  $p$  are not of scientific importance for this study and are simply instrumental factors.**

**Minor comments.**

**Figure 1.** The photolysis laser arguably should be labeled also with 532 nm as some experiments use that wavelength.

Done

**Line 113:** Using the values for the cross section, concentration, and path length for I2 detection, I calculate OD = 0.82.

Apologies, 0.82 is correct, we mistakenly used the path length as 30 cm (the length of the Herriott cell) instead of 40 cm (the length of the single pass cell). This error is only in the specific example in the paper and the correct value of 40 cm was used in the work itself.

**Figure 3.** The caption could be more informative, for example, the time delay between the 248 nm pulse used to initiate the chemistry and the VUV photoionization pulse is not specified. Are the different colored traces the results of measurements at the optimum time for each?

The figure shows a complete time trace, averaged along the time axis, and is only intended to show a clear picture of the species being studied in this experiment, to give the reader an idea of how the peaks appear in the mass spectrum. The caption has been updated to clarify this fact.